IEEE Access
Multidisciplinary : Rapid Review : Open Access Journal

Received August 19, 2021, accepted September 7, 2021, date of publication September 10, 2021, date of current version September 17, 2021.

Digital Object Identifier 10.1109/ACCESS.2021.3111599

The Probe: Design and Development of a Large Hexapod Robot

SANGSIN PARK
IICOMBINED, Seoul 04047, South Korea
e-mail: sangsin80@gmail.com

ABSTRACT A hexapod robot has six legs; as such it can always walk in a statically stable way. In addition, people do not often see large-legged robots in real life. For these reasons, we design and develop a large hexapod robot to impress people at retail stores. The developed hexapod robot, named Probe, has a height of 2.1m, width of 3.3m, and mass of 480kg. The actuator is customized with a frameless BLDC motor, a harmonic drive gear, an electromagnetic brake, a multi-turn absolute magnetic encoder, heat sinks, etc. To firmly secure the frameless motor, we use a clamping ring and suggest the design of a tapered shaft hub and insert. We design an interface circuit board to acquire sensor data and a brake switch board to engage and release brake via an Elmo driver's signal. Additionally, an analytic solution to the kinematic equations of Probe's legs is described. After development of the Probe, Two Probes are deployed at two different stores in South Korea and they conduct scenario motions during business hours. In future, the design of the foot tip will be modified because the urethane cover beneath foot tip wears while the Probe is walking.

INDEX TERMS Actuator design, hexapod robot, legged robot design.

I. INTRODUCTION

As robotic research is maturing, many types of robots are being deployed in various domains. Collaborative robots [1] help workers make products in factories, service robots [2] can assist humans in hospitals, restaurants, and so on, and mobile robots [3] in retail shops can help customers find items or monitor goods for inventory management. The fashion industry is no exception. HRP-4C, a humanoid robot developed at AIST, wore a wedding dress and walked on the runway at the 2009 Yumi Katsura grand collection [4]. Drones flew slowly over the runway, each carrying a bag from Dolce & Gabbana's A/W 2018 women's collection during Milan Fashion Week [5]. Presently, we have unveiled two large hexapod robots named 'Probe' at our eyewear brand (GENTLE MONSTER) retail stores in South Korea. These Probes are presented in Figure 1.

A hexapod robot has six legs and can always walk in a statically stable manner, which means that three legs on the ground perpetually form a supporting polygon while the other three legs are engaged in movement above the floor. That is the most significant reason why I chose a six-legged robot for display at a retail store. Next, because people see few legged robots in real life and do not often see large robots, they will be impressed to see Probe walking.

Studies related to hexapod robots have been widely carried out. The MELMANTIS, a hexapod robot with an integrated limb mechanism, was developed in the mid-1990s [6], [7]. It was able to transform its forelegs into arms. The FZI Research Center for Information Technology has been developing the LAURON series since 1994 and its fifth generation was introduced in 2014 [8]. Each leg of LAURON V had four degrees of freedom(DOF). Accordingly, LAURON V expanded its workspace, walked over steep slope and large obstacles, and manipulated objects using forelegs. A hexapod robot for subsea operations, HexaTerra, was developed at the National Technical University of Athens in Greece [9]. The HexaTerra was driven by an electro-hydraulic actuation system. Another subsea hexapod robot named CRABSTER200 was developed by the Korea Institute of Ocean Science and Technology for seabed investigation and underwater tasks in coastal areas with powerful tidal currents [10], [11]. Its two forelegs had six DOF and were designed for leg-arm transformation. The other four legs had four DOF. Each joint was designed with a customized actuator combined with Kollmorgen frameless bushless DC (BLDC) motors and harmonic gears. Lee *et al.* [12] developed a six-legged robot called the Multi-legged Giant Yardwalker; this robot can

The associate editor coordinating the review of this manuscript and approving it for publication was Giambattista Gruosso.

This work is licensed under a Creative Commons Attribution-NonCommercial-NoDerivatives 4.0 License.
For more information, see https://creativecommons.org/licenses/by-nc-nd/4.0/

(a)

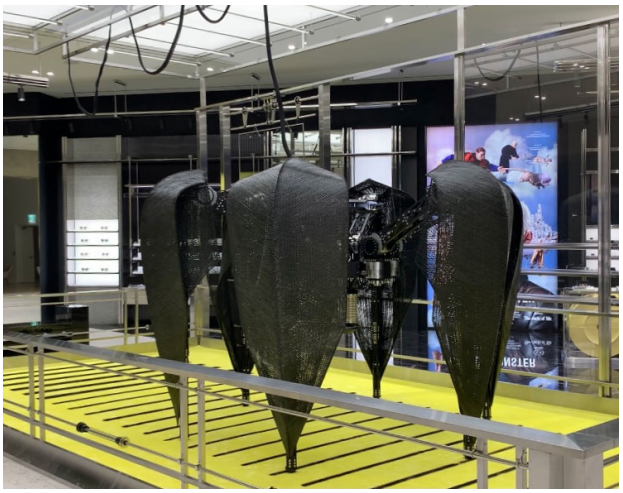

(b)

FIGURE 1. (a) The first Probe at HAUS DOSAN store and (b) the second Probe at the Starfield Hanam store were deployed in February and June 2021, respectively.

transform its leg configuration to change its body height. Faudzi *et al.* [13] developed a long, light and thin legged hexapod robot named Giacometti robot. They developed a thin soft McKibben muscle which is a pneumatic artificial muscle for Giacometti robot's thin legs. Chen *et al.* [14] presented a hexapod robot which can rearrange legs around its body.

In DLR, a small hexapod robot, DLR-Crawler, was developed by using the fingers of DLR-Hand II [15]. It used to be an equipment for the evaluation of locomotion control algorithms in the uneven terrain and the different position-based and force-based leg. A hexapod named Weaver was developed by Bjelonic *et al.* [16]. They combined proprioceptive and exteroceptive sensing to improve the terrain perception for autonomous navigation of Weaver on outdoor terrain. Minati *et al.* [17] proposed an approach to joint motor pattern generation based on a hierarchical network of coupled nonlinear oscillators arranged over two levels, and they verified it using a hexapod robot. Travers *et al.* [18] focused on rough terrain locomotion, and designed a two-layered control scheme to adapt to climb over a variety of steps and ledges. They demonstrated that a series-elastic actuated hexapod robt climbed over different obstacles. Tam *et al.* with CSIRO's Robotics and Autonomous Systems Group developed Open-source Syropod High-level Controller (OpenSHC) which is a controller for multilegged robots to generate statically stable gaits [19]. For a hexapod robot, Belter and Skrzypczyński [20] developed feasible gait patterns using evolutionary algorithm with dependencies inspired by typical insect behaviour.

My contributions related to actuator development are that I design a joint module consisting of a frameless BLDC motor, harmonic drive, electric brake, and absolute contactless encoder for a revolute joint, as well as introducing an adhesive-free design for tightening rotor of frameless motor and a drive shaft. Furthermore, based on the actuator design, I develop the Probe (a large hexapod robot) with a mass of 480kg and height of 2.1m. All mechanical and electronic parts (e.g., actuator, leg, body, and exterior parts, electronic circuit boards, wire harnesses, etc.) are fabricated in the laboratory. Another contribution is that I present an example of a legged robot application in the real world. Since the first and second deployments in February and June 2021, respectively, the Probe has shown people its walking like a fashion model at our retail shop. The Probe's walking can make people interested and visit at our retail shops. Also, we have a plan to show a third Probe in Shanghai in September 2021.

The paper is organized as follows. Section 2 provides the hardware design including details of the actuator, legs, and electronic circuit boards. The inverse kinematics of the Probe is described in Section 3 and gait strategy is presented in Section 4. In Sections 5, experiment results are presented and results of installations at retail stores are shown in section 6. Finally, discussion and conclusions are described in Sections 7 and 8, respectively.

II. HARDWARE DESIGN

The aims of robot design are for people to be impressed by the size of the robot and for robot to walk stably at a store during business hours (about 10 hours) every day. Thus, I have developed a large hexapod robot named Probe. Except for exterior parts on legs, its standing posture is a height of 2.0m, width of 2.7m, and mass of 427kg. Moreover, with exterior parts on legs, it has a height of 2.1m, width of 3.3m, and mass of 480kg. The robot design with and without exterior parts are presented in Figures 2 and 3, respectively.

The hardware specifications of Probe with exterior parts are summarized in Table 1. Each leg has three DOF; total DOF of Probe are eighteen. Designed actuators, which include a frameless BLDC motor and harmonic drive gear, are applied at each joint. For real-time control, a Xenomai-patched Linux kernel is implemented on Ubuntu 16.04; the control frequency is 250Hz. A USB camera is applied for

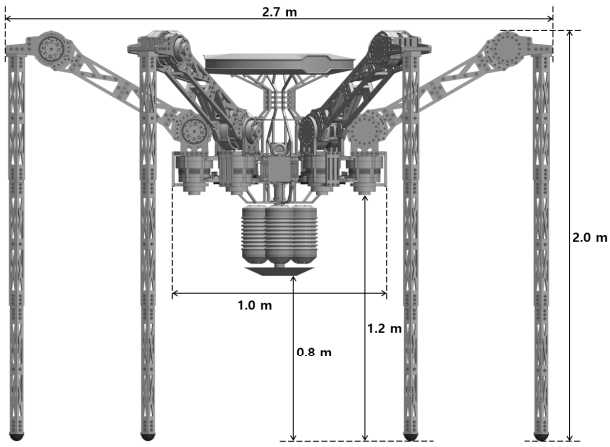

FIGURE 2. Mechanical design of Probe without exterior parts. Maximum width is 2.7m, height is 2.0m, and shortest length from ground is 0.8m. This configuration is body-up posture before walking.

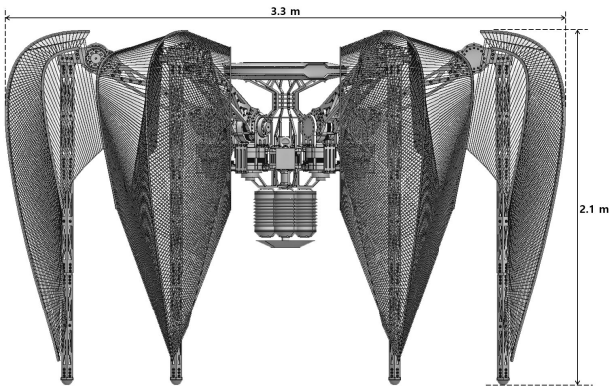

FIGURE 3. Probe with exterior parts on legs in body-up posture. Maximum width is 3.3m and height is 2.1m.

adjusting the position and rotation of Probe when it comes back to the starting point.

A. DESIGN OF ACTUATOR

I design actuators for all revolute joints, as presented in Figure 4. The actuator contains a frameless BLDC motor, harmonic drive gear, electromagnetic brake, multi-turn absolute magnetic encoder, housing components, drive shaft and shaft hub components for tightening motor rotor, etc. To transfer heat generated by BLDC motor to the open-air, six heat sink blocks are placed around stator of motor. Thermal pads between the heat sinks and the stator are applied to improve the heat sink performance. I employ the electromagnetic brake to allow Probe to stand up and the absolute encoder to memorize the current joint angle after shutting down. Each brake is connected to a brake controller and brake controllers are synchronized with motor drivers, i.e. if motor is in operation, the brake is released automatically.

A frameless motor is used to customize robotic joints. Thus, design approaches are needed to clamp the motor stator and housing and secure the motor rotor firmly to the drive shaft. In the case of the stator, referring to Kollmorgen's mounting and installation guidelines [21], it is fastened to the housing using a clamp ring. On the other hand, in the case of the rotor, I suggest a design approach to secure it firmly without using any adhesives. Components of rotor module are shown in Figure 5 and a cross section of the rotor module is presented in Figure 6. A shaft hub, an inner-tapered cylinder, is placed between rotor yoke and shaft. A tapered insert fitting inside the shaft hub, and the shaft, are bolted together. With more bolting, the tapered insert moves deeper, and then the outer surface of the shaft hub presses more against the rotor yoke.

TABLE 1. Hardware specifications of Probe.

Mass	480kg
Height	2.1m
Width	3.3m
Degrees of freedom	18 (6 legs × 3 DOF per leg)
Motor	KOLLMORGEN frameless BLDC motor 830W, 48V
Speed reducer	Leaderdrive® harmonic drive gear 120:1
Brake	OGURA electromagnetic spring-applied brake
Motor driver	ELMO Gold Solo Twitter
Sensor	RENISHAW Orbis™ true absolute rotary encoder × 18 ANALOG DEVICES 6-axis IMU × 1 USB camera × 1
Communication	CAN 2.0A
PC	INTEL® NUC8i5BEH × 1 CPU i5-8259U, 2.3GHz RAM 16GB, SSD 256GB
OS	Ubuntu 16.04 based on a Xenomai-patched Linux kernel
Supply voltages	48V for motor driver 24V for others

B. DESIGN OF LEG

Based on the customized actuator, the leg of the Probe is designed as an RRR configuration and is shown in Figure 7. From the body side, the three joints are named as the hip yaw, hip pitch, and knee joint, sequentially. The six trapezoid prisms of the shank are placed next to each other to make a hexagonal outline; a hexagonal ring inside them increases the stiffness of the shank. The shank is divided into three segments and, from segment 1 to segment 3, the diameter of segment contour becomes narrower. Then, the shank is tapered at the foot tip. Moreover, urethane covers beneath the foot tips are applied to decrease slip of legs and impact when legs touch down.

C. DESIGN OF ELECTRONIC CIRCUIT BOARDS

I design an interface circuit board; its block diagram is shown in Figure 8. A STM32F413VGT is used for MCU and a buzzer is on the board as an audio indicator. The main functions of the interface board are to acquire the data of the IMU fixed beneath the interface board through SPI and the data of the photoelectric sensors installed on the fence through

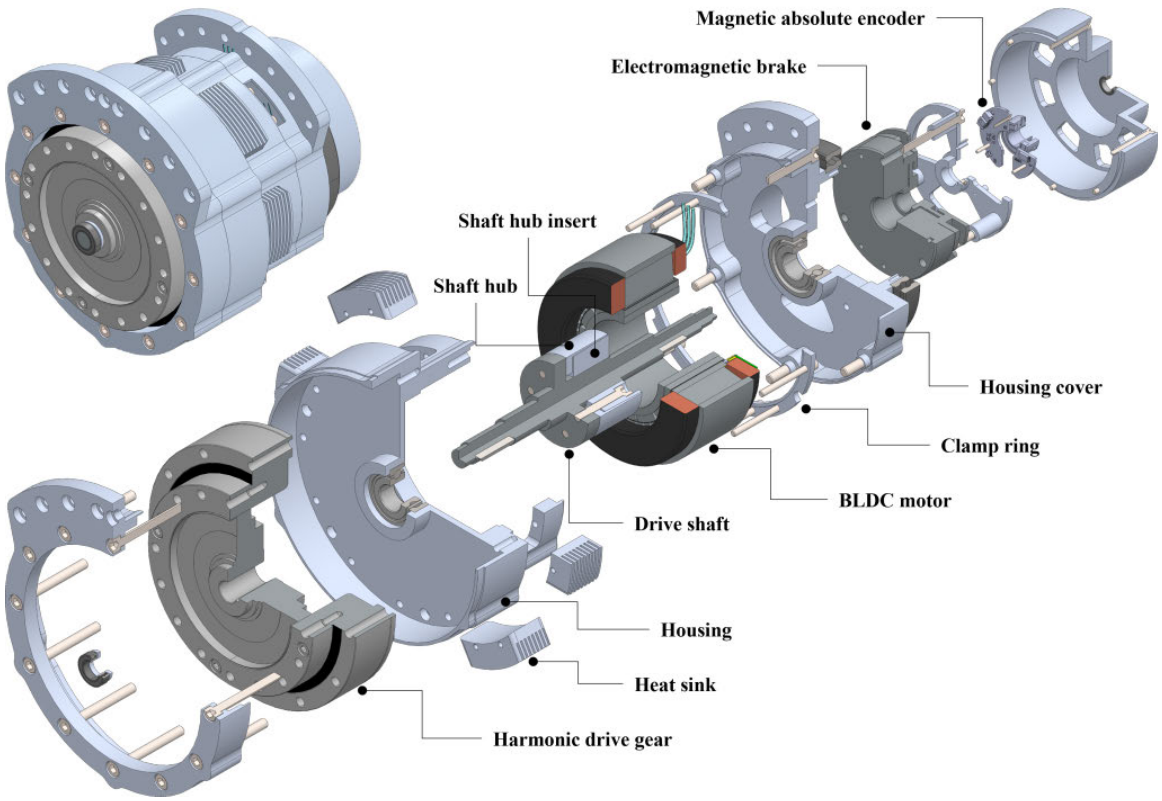

FIGURE 4. An assembled actuator is placed at top left and it breaks down as follows: a harmonic drive gear, housing, drive shaft, shaft hub, shaft hub insert, BLDC motor, clamp ring, electromagnetic brake, magnetic absolute encoder, six heat sinks, etc. All parts except for a drive shaft are made of aluminium alloy and the drive shaft is made of stainless steel.

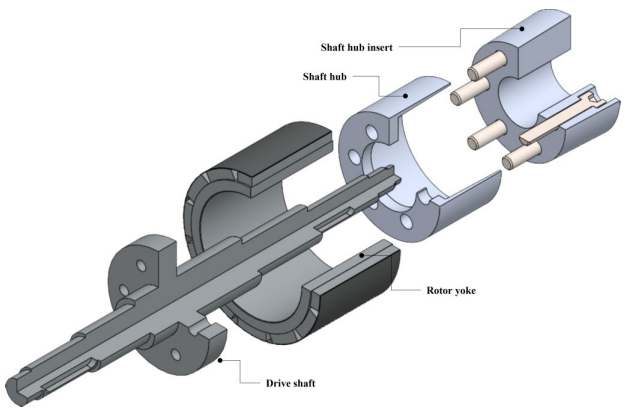

FIGURE 5. A rotor module consists of a drive shaft, motor rotor, shaft hub, and shaft hub insert.

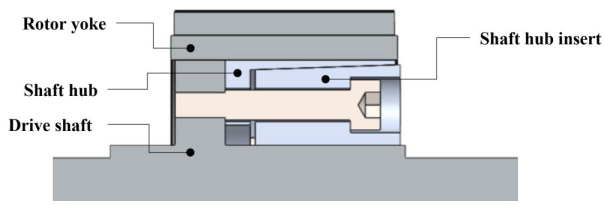

FIGURE 6. This is a cross section of an assembled rotor module. Because of an inner-tapered cylinder and tapered insert, a rotor yoke and drive shaft are secured firmly together after bolting.

RS232C. Also, the interface circuit board can be the 24V power distributor for the electromagnetic brakes and the CAN bus hub. The odd-numbered legs (leg_1, leg_3, and leg_5) are connected to the channel 1 CAN bus, and the even-numbered legs (leg_2, leg_4, and leg_6) to the channel 2 bus.

Next, for engaging and releasing brake, I also design the brake switch board; its schematic is presented in Figure 9. The brake can be engaged or released through a solid state relay (SSR) as well as a manual toggle switch. Thus, by means of connection to each Elmo motor driver, each brake switch board is synchronized with the Elmo driver's digital output signal.

The assembled PCBs of an interface circuit board and a brake switch board are shown in Figure 10. The IMU is combined at the bottom of the interface circuit board. The brake switch board consists of two PCBs; they are connected by pin headers. All connectors are on the top PCB and an SSR and manual toggle switch are on the bottom PCB.

III. INVERSE KINEMATICS

Following the standard Denavit and Hartenberg (DH) convention, the coordinate frames for the nth leg are presented in Figure 11. The body fixed frame, hip base frame, hip yaw

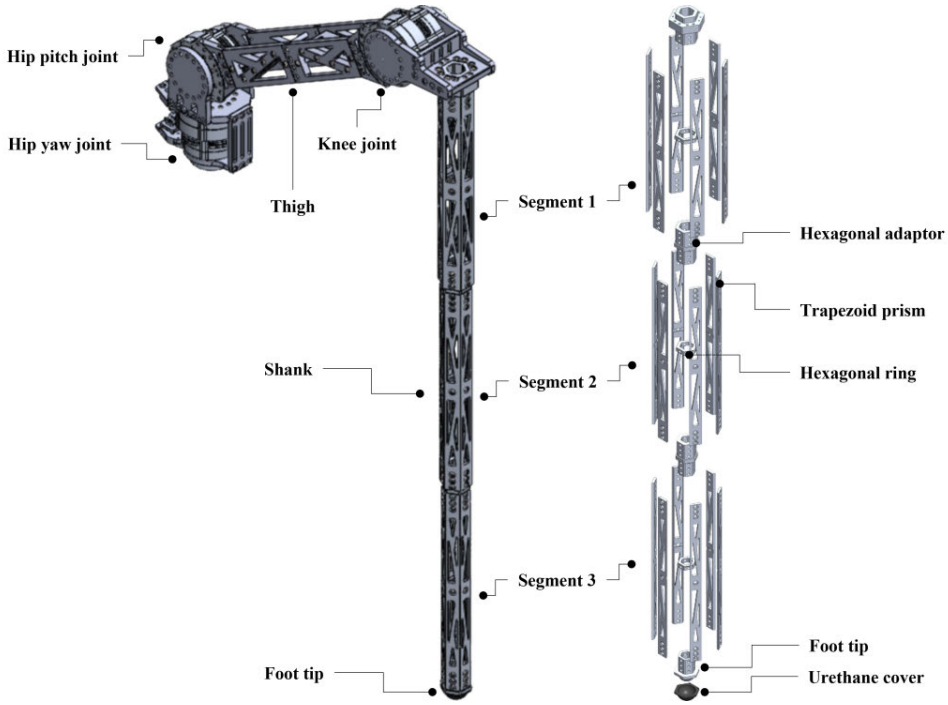

FIGURE 7. A leg has three DOF and the shank is longer than the thigh. To make the shank longer, three segments are connected with hexagonal adaptors. Urethane covers beneath foot tips can absorb touch-down shock.

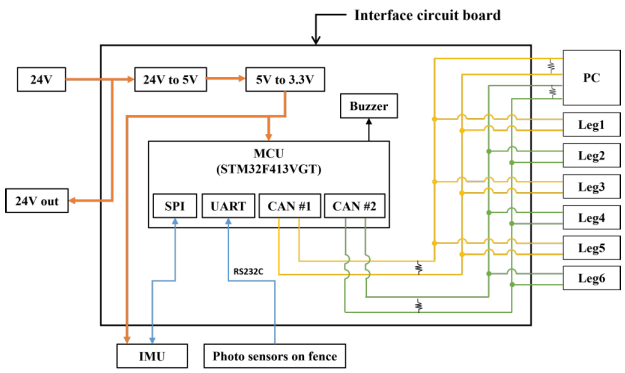

FIGURE 8. Block diagram of an interface circuit board.

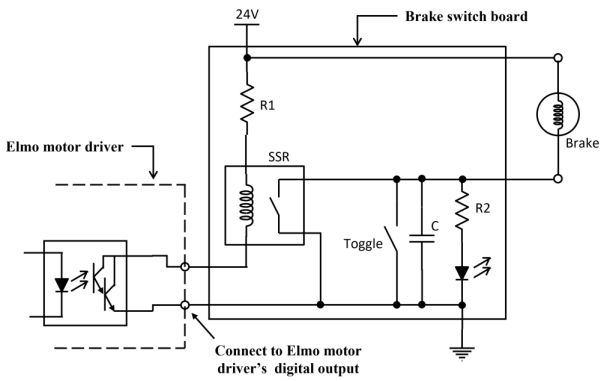

FIGURE 9. Elmo motor driver controls electromagnetic brake via brake switch board.

frame, hip pitch frame, knee frame, and foot frame are placed sequentially. q_h, q_{hy}, q_{hp}, and q_{kn} are hip base angle with respect to the body fixed frame, hip yaw angle with respect to the hip base frame, hip pitch angle with respect to the hip yaw frame, and knee angle with respect to the hip pitch frame, respectively. Also, l_0, l_1, l_2, l_3, and l_4 are the length between the body fixed frame and the hip base frame, the vertical offset length from the hip base frame to the hip yaw frame, the thigh length, the offset between the hip pitch frame and the knee frame, and a shank length, respectively. The legs are positioned equally along the body contour. Thus, q_h of the leg$_i$ (i=1, …, 6) are 0, $\pi/3$, $2\pi/3$, π, $4\pi/3$, and $5\pi/3$, respectively. From the coordinate frames, the DH parameters for the nth leg are derived and shown in Table 2.

TABLE 2. DH parameters for n^{th} leg.

i	θ_i	α_i	a_i	d_i
h	q_h	0	l_0	0
hy	q_{hy}	$-\frac{\pi}{2}$	0	l_1
hp	q_{hp}	0	l_2	0
kn	q_{kn}	0	l_3	0
f	$\frac{\pi}{2}$	0	l_4	0

Based on Table 2, the five homogenous transformation matrices are equal to

$$ {}^{c}T_h = \begin{bmatrix} c_h & -s_h & 0 & l_0 c_h \\ s_h & c_h & 0 & l_0 s_h \\ 0 & 0 & 1 & 0 \\ 0 & 0 & 0 & 1 \end{bmatrix}, $$

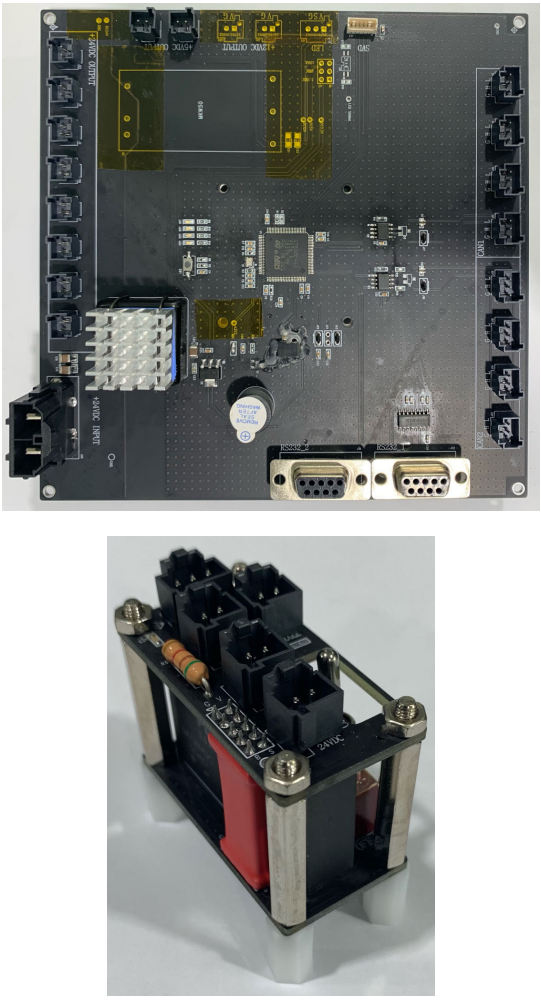

FIGURE 10. Assembled PCB of interface circuit board is at left side and assembled brake switch board PCB at right side.

$$
{}^{h}T_{hy} = \begin{bmatrix} c_{hy} & 0 & -s_{hy} & 0 \\ s_{hy} & 0 & c_{hy} & 0 \\ 0 & -1 & 0 & l_1 \\ 0 & 0 & 0 & 1 \end{bmatrix},
$$

$$
{}^{hy}T_{hp} = \begin{bmatrix} c_{hp} & -s_{hp} & 0 & l_2 c_{hp} \\ s_{hp} & c_{hp} & 0 & l_2 s_{hp} \\ 0 & 0 & 1 & 0 \\ 0 & 0 & 0 & 1 \end{bmatrix},
$$

$$
{}^{hp}T_{kn} = \begin{bmatrix} c_{kn} & -s_{kn} & 0 & l_3 c_{kn} \\ s_{kn} & c_{kn} & 0 & l_3 s_{kn} \\ 0 & 0 & 1 & 0 \\ 0 & 0 & 0 & 1 \end{bmatrix},
$$

$$
{}^{kn}T_{f} = \begin{bmatrix} 0 & -1 & 0 & 0 \\ 1 & 0 & 0 & l_4 \\ 0 & 0 & 1 & 0 \\ 0 & 0 & 0 & 1 \end{bmatrix}, \tag{1}
$$

where $c_h = \cos q_h$, $s_h = \sin q_h$, $c_{hy} = \cos q_{hy}$, $s_{hy} = \sin q_{hy}$, $c_{hp} = \cos q_{hp}$, $s_{hp} = \sin q_{hp}$, $c_{kn} = \cos q_{kn}$, and $s_{kn} = \sin q_{kn}$. The vector from the body fixed frame to the foot frame is

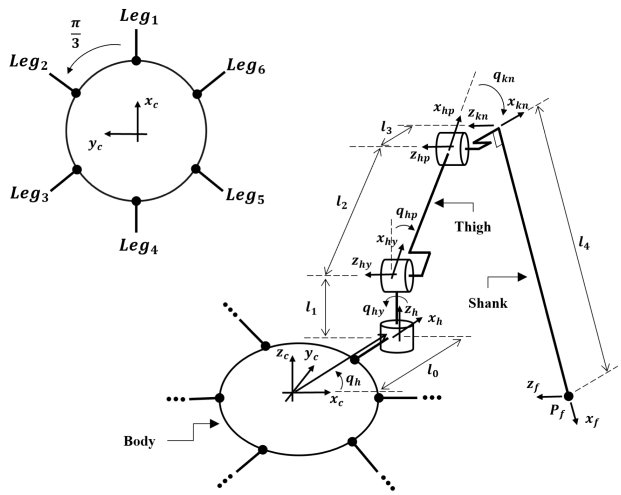

FIGURE 11. Coordinate frames for Probe legs.

the same as the sum of one vector from the body fixed frame to the hip base frame and another vector from the hip base frame to the foot frame. Since the one vector from the body fixed frame to the hip base frame is constant, I use the another vector from the hip base frame to the foot frame to derive an analytic solution of the kinematic equations. Based on Eq. (1), the foot frame with respect to the hip base frame is given by

$$
\begin{aligned}
{}^{h}T_{f} &= {}^{h}T_{hy}\,{}^{hy}T_{hp}\,{}^{hp}T_{kn}\,{}^{kn}T_{f} \\
&= \begin{bmatrix} -c_{hy}s_{hpkn} & -c_{hy}c_{hpkn} & -s_{hy} & P_{f,x} \\ -s_{hy}s_{hpkn} & -s_{hy}c_{hpkn} & c_{hy} & P_{f,y} \\ -c_{hpkn} & s_{hpkn} & 0 & P_{f,z} \\ 0 & 0 & 0 & 1 \end{bmatrix},
\end{aligned} \tag{2}
$$

where $c_{hpkn} = \cos(q_{hp} + q_{kn})$ and $s_{hpkn} = \sin(q_{hp} + q_{kn})$. From the fourth column of Eq. (2), the x, y, and z positions of the foot are derived and I call them $P_{f,x}$, $P_{f,y}$, and $P_{f,z}$, respectively. Then, Eq. (2) can be summarized as three kinematic equations,

$$
P_{f,x} = -l_4 c_{hy} s_{hpkn} + l_3 c_{hy} c_{hpkn} + l_2 c_{hy} c_{hp} \tag{3}
$$

$$
P_{f,y} = -l_4 s_{hy} s_{hpkn} + l_3 s_{hy} c_{hpkn} + l_2 s_{hy} c_{hp} \tag{4}
$$

$$
P_{f,z} = -l_4 c_{hpkn} - l_3 s_{hpkn} - l_2 s_{hp} + l_1. \tag{5}
$$

Throughout inverse kinematics process, the analytic solutions to Eq. (3), (4), and (5) are derived as

$$
q_{hy} = \tan^{-1} \frac{P_{f,y}}{P_{f,x}} \tag{6}
$$

$$
q_{hp} = \tan^{-1} \frac{s_{hp}}{c_{hp}} \tag{7}
$$

$$
q_{kn} = \tan^{-1} \frac{-l_3 k_6 - l_4 k_5}{l_3 k_5 - l_4 k_6}, \tag{8}
$$

where,

$$
\begin{aligned}
k_1 &= P_{f,x}/c_{hy}, \\
k_2 &= l_1 - P_{f,z}, \\
k_3 &= (l_2^2 + l_3^2 + l_4^2 - k_1^2 - k_2^2)/2l_2,
\end{aligned}
$$

$$
\begin{aligned}
k_4 &= l_2 - k_3, \\
k_5 &= k_1 c_{hp} + k_2 s_{hp} - l_2, \\
k_6 &= k_1 s_{hp} - k_2 c_{hp}, \\
c_{hy} &= \cos q_{hy}, \\
c_{hp} &= (\, k_4 k_1 + k_2 \sqrt{k_1^2 + k_2^2 - k_4^2}\,)/(\, k_1^2 + k_2^2\,), \\
&\text{and } s_{hp} = -\sqrt{1 - c_{hp}^2}.
\end{aligned}
$$

Therefore, when the foot coordinates are given, the joint angles can be determined using the analytic solutions of Eqs. (6), (7), and (8). Regarding the process of inverse kinematics, further details are provided in Appendix.

IV. TRIPOD GAIT

The tripod gait algorithm, which ensures that the three legs on the ground while the other three legs swing, is implemented on the Probe. The gait scheme is presented in Figure 12. Legs are grouped into odd-numbered legs (leg_1, leg_3, and leg_5), OL, and even-numbered legs (leg_2, leg_4, and leg_6), EL. When the Probe is supported by either OL or EL, I call the status single support phase (SSP), and when the Probe is supported by both OL and EL, I call the status double support phase (DSP). DSP sequences of the tripod gait are as follows; $(OL_0, EL_0) \rightarrow (OL_1, EL_0) \rightarrow (OL_1, EL_1) \rightarrow (OL_2, EL_1) \cdots$. Initially, the Probe is supported by both OL and EL (DSP state). When starting a forward walk, the OL swings forward, the EL still supports the Probe (SSP state) and meanwhile, the body moves forward with constant velocity. After the OL touches down, the Probe is supported by all legs again (DSP state); in the meantime, the body keeps moving forward constantly. At the end of all-leg support, the set of swing legs changes to the EL and the OL keeps supporting the Probe (SSP state). Therefore, the gait begins every period by alternating between OL and EL.

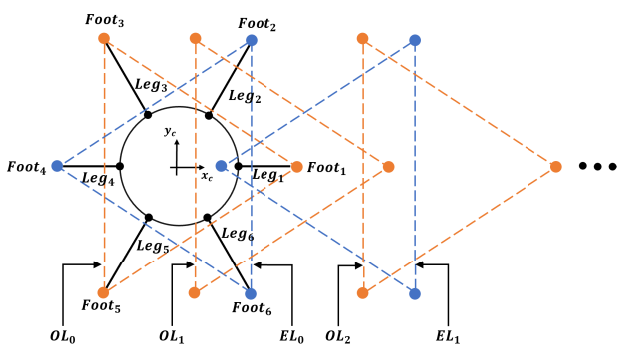

FIGURE 12. DSP sequences of the tripod gait for forward walking: $(OL_0, EL_0) \rightarrow (OL_1, EL_0) \rightarrow (OL_1, EL_1) \rightarrow (OL_2, EL_1) \cdots$. When SSP, either OL or EL makes a triangular supporting area. When DSP, both OL and EL make a hexagonal supporting area.

For example, I can think about walking twelve steps forward with a walking period of 3.2s (SSP of 1.92s and DSP of 1.28s), a step length of 26cm, and a height of foot lift of 4.5cm. Then, the x, y, and z coordinates of each leg's foot are presented in Figures 13, 14, and 15. In the forward walking case, the y coordinate of each leg's foot stays in the initial position.

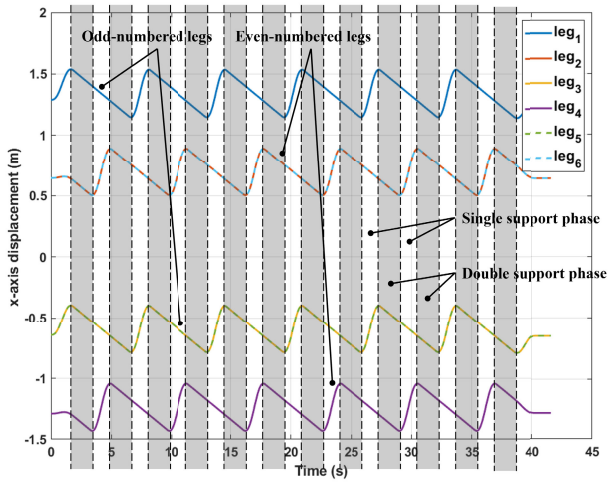

FIGURE 13. Each grey area is DSP in each walking period. While DSP, body of the Probe moves constantly. Displacements of $foot_2$ and $foot_6$ are identical and displacements of $foot_3$ and $foot_5$ overlap.

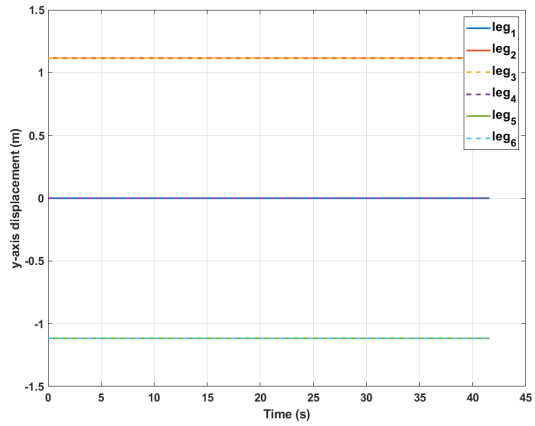

FIGURE 14. Each leg's position is maintained for forward walking.

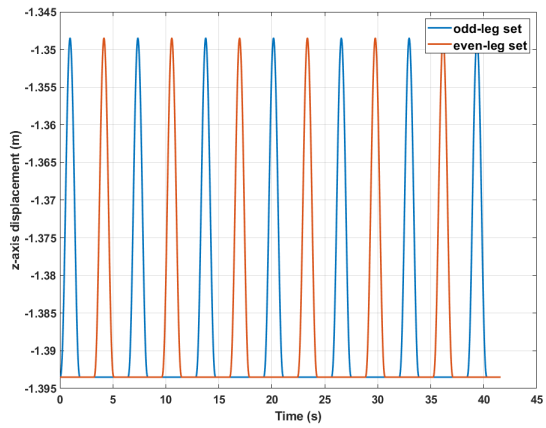

FIGURE 15. While walking, sets of feet alternate between odd-numbered legs and even-numbered legs and moves simultaneously.

V. EXPERIMENT RESULTS

A USB camera is used to make the Probe adjust its position and rotation at the end of backward walking. The camera is installed at a bottom part of the Probe's body and a black square marker (8cm × 8cm) is used to make starting position and is placed under the camera. Then, the camera detects the edge of the marker. The installation and the camera image are illustrated in Figure 16. A resolution of the camera image is 320 × 240 pixels. To detect the edge of the marker, I adopt OpenCV's functions: a "GaussianBlur" for image smoothing, "Canny" for edge detection, and "findContours" for finding contours.

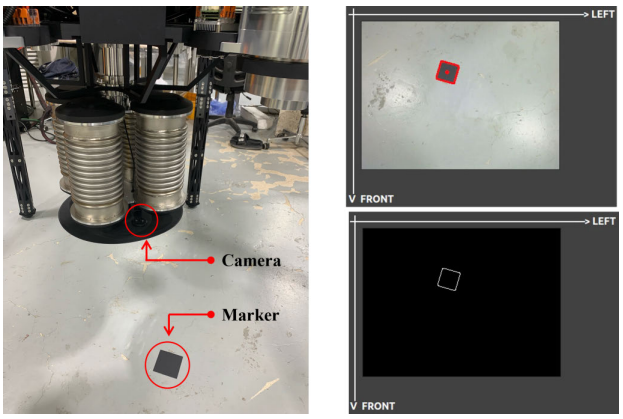

FIGURE 16. A camera is installed at a bottom part of the Probe's body and a black square marker is placed under the camera. A camera image and the detected edge is shown in a right side.

To explain a strategy for returning to the starting position, I call the scenario a sequence of the Probe's motions from now on. The camera memorizes position and rotation of the edge before the first scenario for a reference and calculates position and rotation differentials between the memorized edge and the edge detected after each scenario. Then, the Probe can move and rotate to compensate the differentials.

The results of an adjustment to the starting position after eleven scenarios are illustrated in Figure 17. A red square and a red dot are the edge of the starting position and the center of it, respectively. Blue squares and blue dots are the detected edges and the centers of them after scenarios, respectively. The root-mean-square deviation (RMSD) of X-position of the blue dots is 2.149 pixel, the RMSD of Y-position of them is 2.294 pixel and the RMSD of rotation angle of the blue squares is 0.279°.

VI. INSTALLATION RESULTS

Two Probes are installed at the HAUS DOSAN store and the Starfield Hanam store. An installation diagram of the implemented system is illustrated in Figure 18. For safety, the Probe is surrounded by metal fences and is not allowed to step out of dual boundaries: a physical boundary and an invisible boundary made by four photoelectric sensors. If the Probe touches the invisible boundary, remaining scenarios are promptly ignored, and the Probe keeps staying at the starting

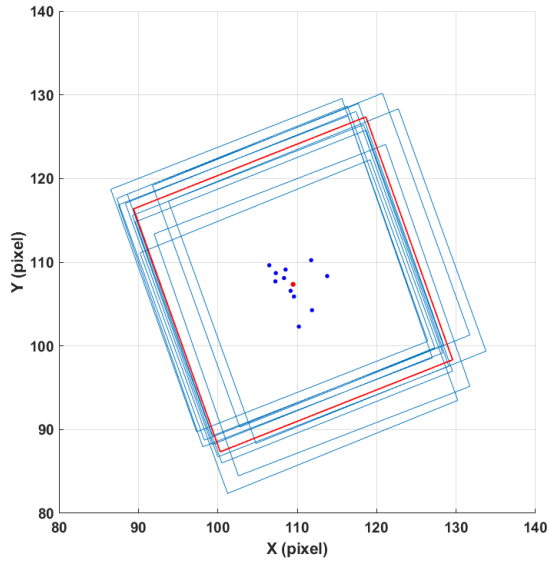

FIGURE 17. The edges of the marker and the centers of them. A red square and a red dot are the reference edge and the center of it, respectively. Blue squares and blue dots are the detected edges and the centers of them, respectively.

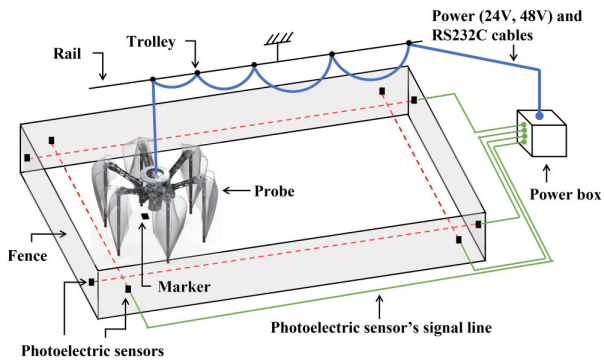

FIGURE 18. An installation diagram of the implemented system. The Probe is surrounded by metal fences and they makes a physical boundary. Particularly, an invisible boundary made by four photoelectric sensors is indicated by red dotted lines. Digital signals of the photoelectric sensors are encoded in a power box, and an encoded byte is sent to the Probe through RS232C serial communication. Power cables and a RS232C cable are connected to trolleys that runs on a suspended rail.

position. It is wired with a power box for continuous power and RS232C serial communication.

They are not autonomous but conduct a set of predefined motions repeatedly during business hours (about 10 hours). The sequence of motions is as follows: body move-up, forward walking, move-down, move-up, backward walking, adjustment to starting position, and move-down. In Figures 19 and 20, parts of the scenario are shown.

VII. DISCUSSION

At the beginning of conceptual design, the Probe was a walking showroom to display eyewear outside. Thus, its height and width were 2.4m and 4.0m, respectively, and it carried a

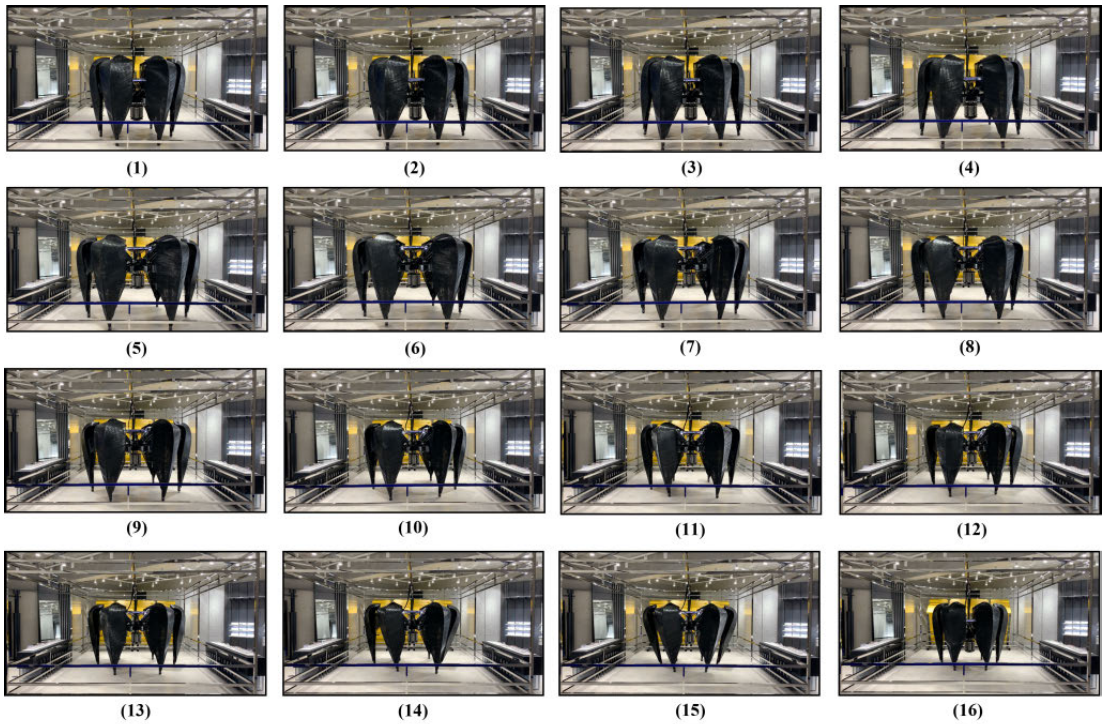

FIGURE 19. Part of scenario in HAUS DOSAN store. From (1) to (4), the Probe moves its body up; then from (5) to (12), it walks forward. From (13) to (16), its body goes down.

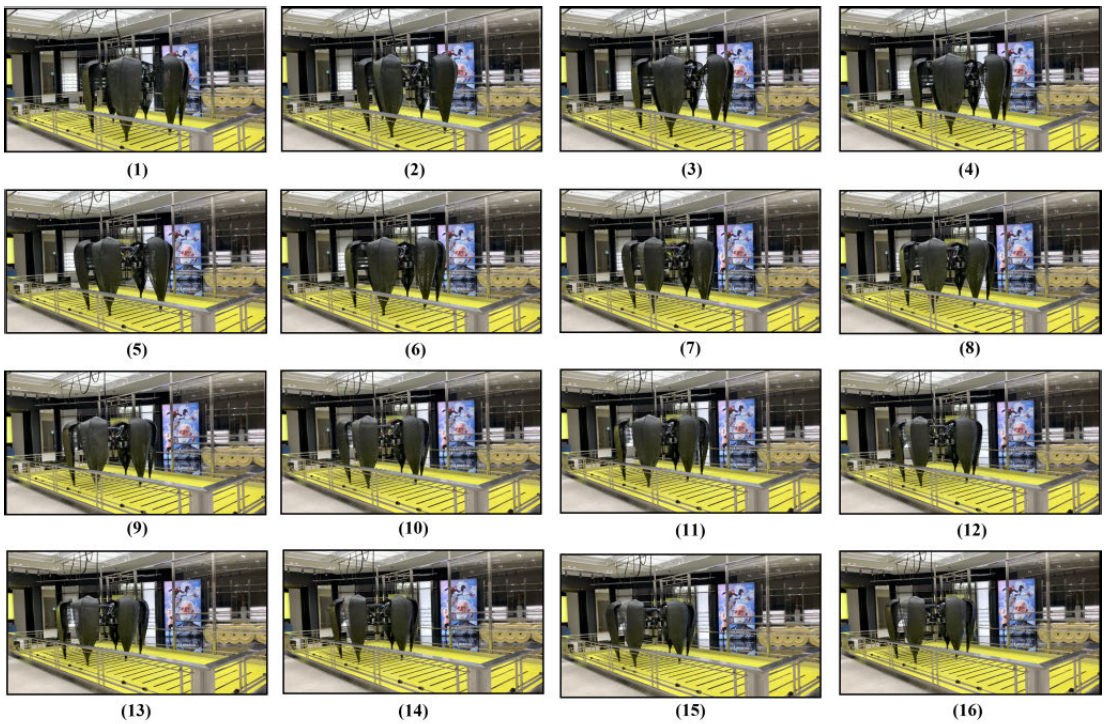

FIGURE 20. Part of scenario in Starfield Hanam store. From (1) to (16), the Probe walks backward.

payload of 80kg. As its name implies, we also considered that the Probe would explore the unknown places and pretend to investigate soil, rocks, etc. like the Mars exploration rovers. After design discussion, however, we decided that the Probe would be operated in retail stores, then I modified its size as a height of 2.0m and width of 2.7m.

While operating the first Probe at the HAUS DOSAN store, I found a minor issue. The urethane covers beneath the foot tips are worn a lot. A sample of a worn urethane cover is shown in Figure 21. While the Probe's body is supported by its legs and moves forward and backward, each supporting leg rotates around its foot tip; then, the urethane covers are easily damaged. Thus, the foot tip needs to be modified to add a free-rotation joint. Currently, to solve this issue, I replace the worn urethane cover with a new one.

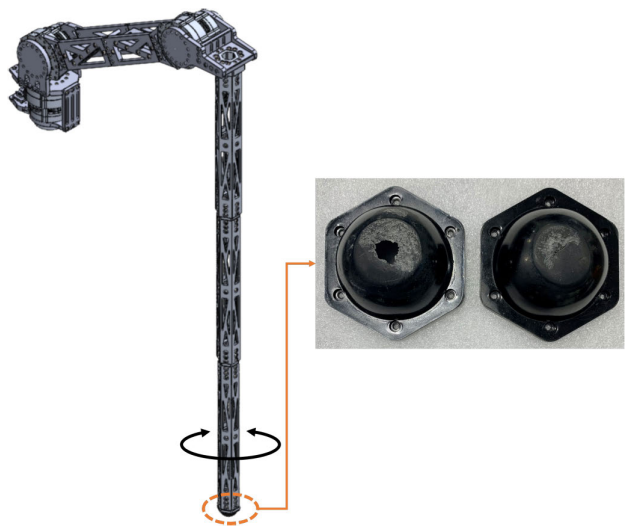

FIGURE 21. Sample of worn urethane covers. Left one is worst case, with hole.

VIII. CONCLUSION

This paper describes the design and development of a large hexapod robot named Probe which has a height of 2.1m, width of 3.3m, and mass of 480kg. Actuator is designed for all joints of the Probe. It consists of a frameless BLDC motor, a harmonic drive gear, an electromagnetic brake, a multi-turn absolute magnetic encoder, etc. Six heat sink blocks are placed around a stator of the motor and a clamping ring is used to tighten the motor stator. To secure the motor rotor firmly to the drive shaft, a tapered shaft hub and insert are designed. The leg of the Probe is designed as an RRR configuration. The shank is divided into three segments. The shank is tapered at the foot tip. Each segment of the shank consists of six trapezoid prisms to make a hexagonal outline. To decrease slip of leg and impact force, a urethane cover is applied beneath each foot tip. An interface circuit board is implemented to acquire the data of the IMU fixed beneath the interface board through SPI and the data of photoelectric sensors installed on the fence through RS232C. The brake switch board is designed for engaging and releasing brake via an Elmo driver's signal. An analytic solution of the leg's RRR configuration is derived and exact joint angles can be calculated when walking pattern is given. Additionally, a camera is implemented to adjust the position and rotation of the Probe at the end of backward walking. As a result, two Probes are installed at two different stores in South Korea and they conduct predefined motions during business hours.

While operating the first Probe, a minor issue, that urethane covers are worn, is raised. Currently, I solve the issue by replacing the worn urethne covers with new ones. In future, the design of the foot tip will be modified.

ACKNOWLEDGMENT

The author would like to thank his employer Hankook Kim and his supervisor Jonggyu Jang for their consistent support. Furthermore, he would like to thank his team member Jae-hyun Lee for fabrication of the Probe and his assistance.

APPENDIX

A. ANGLE OF HIP YAW JOINT

Eq. (3) multiplied by s_{hy} is

$$P_{f,x}s_{hy} = -l_4c_{hy}s_{hpkn}s_{hy} + l_3c_{hy}c_{hpkn}s_{hy} + l_2c_{hy}c_{hp}s_{hy}. \quad (9)$$

Eq. (4) multiplied by c_{hy} is

$$P_{f,y}c_{hy} = -l_4s_{hy}s_{hpkn}c_{hy} + l_3s_{hy}c_{hpkn}c_{hy} + l_2s_{hy}c_{hp}c_{hy}. \quad (10)$$

Then, Eq. (10) subtracted from Eq. (9) is

$$P_{f,x}s_{hy} - P_{f,y}c_{hy} = 0. \quad (11)$$

Therefore,

$$q_{hy} = \tan^{-1}\frac{P_{f,y}}{P_{f,x}}. \quad (12)$$

B. ANGLE OF HIP PITCH JOINT

Eq. (3) multiplied by c_{hy} is

$$P_{f,x}c_{hy} = -l_4c_{hy}^2s_{hpkn} + l_3c_{hy}^2c_{hpkn} + l_2c_{hy}^2c_{hp}. \quad (13)$$

Eq. (4) multiplied by s_{hy} is

$$P_{f,y}s_{hy} = -l_4s_{hy}^2s_{hpkn} + l_3s_{hy}^2c_{hpkn} + l_2s_{hy}^2c_{hp}. \quad (14)$$

Then, Eq. (14) added to Eq. (13) is

$$l_2c_{hp} - l_4s_{hpkn} + l_3c_{hpkn} = k_1, \quad \text{where } k_1 = P_{f,x}/c_{hy}. \quad (15)$$

Rewriting Eq. (5) as an equation,

$$l_2s_{hp} + l_4c_{hpkn} + l_3s_{hpkn} = k_2, \quad \text{where } k_2 = l_1 - P_{f,z}. \quad (16)$$

Eq. (15) squared equals

$$l_2^2c_{hp}^2 + (l_4s_{hpkn} - l_3c_{hpkn})^2 - 2l_2c_{hp}(l_4s_{hpkn} - l_3c_{hpkn}) = k_1^2. \quad (17)$$

Eq. (16) squared equals

$$l_2^2s_{hp}^2 + (l_4c_{hpkn} + l_3s_{hpkn})^2 + 2l_2s_{hp}(l_4c_{hpkn} + l_3s_{hpkn}) = k_2^2. \quad (18)$$

Then, Eq. (18) added to Eq. (17) is

$$l_2^2 + l_4^2 + l_3^2 - 2l_2(l_4s_{kn} - l_3c_{kn}) = k_1^2 + k_2^2. \quad (19)$$

Rewriting Eq. (19) as

$$l_4 s_{kn} - l_3 c_{kn} = k_3, \quad \text{where } k_3 = (l_2^2 + l_3^2 + l_4^2 - k_1^2 - k_2^2)/2l_2. \tag{20}$$

Next, Eq. (15) multiplied by c_{hp} is

$$l_2 c_{hp}^2 - l_4 s_{hpkn} c_{hp} + l_3 c_{hpkn} c_{hp} = k_1 c_{hp}. \tag{21}$$

Eq. (16) multiplied by s_{hp} is

$$l_2 s_{hp}^2 + l_4 c_{hpkn} s_{hp} + l_3 s_{hpkn} s_{hp} = k_2 s_{hp}. \tag{22}$$

Then, Eq. (22) added to Eq. (21) is

$$l_2 - l_4 s_{kn} + l_3 c_{kn} = k_1 c_{hp} + k_2 s_{hp}. \tag{23}$$

Substitute Eq. (20) into Eq. (23) and rewrite the equation as

$$k_2 s_{hp} = k_4 - k_1 c_{hp}, \text{ where } k_4 = l_2 - k_3. \tag{24}$$

Eq. (24) squared equals

$$k_2^2 s_{hp}^2 = k_4^2 - 2k_4 k_1 c_{hp} + k_1^2 c_{hp}^2. \tag{25}$$

Substitue $s_{hp}^2 = 1 - c_{hp}^2$ into Eq. (25) and rewrite the result as

$$(k_1^2 + k_2^2) c_{hp}^2 - 2k_4 k_1 c_{hp} + k_4^2 - k_2^2 = 0. \tag{26}$$

Then, the solutions of Eq. (26) are

$$c_{hp} = (k_4 k_1 + k_2\sqrt{k_1^2 + k_2^2 - k_4^2})/(k_1^2 + k_2^2) \text{ or } (-k_4 k_1 + k_2\sqrt{k_1^2 + k_2^2 - k_4^2})/(k_1^2 + k_2^2), \tag{27}$$

but the first is only used for calculating the hip pitch angle.

Therefore, from Eq. (27),

$$q_{hp} = \tan^{-1} \frac{s_{hp}}{c_{hp}}, \text{ where } s_{hp} = -\sqrt{1 - c_{hp}^2}. \tag{28}$$

C. ANGLE OF KNEE JOINT

Rewriting Eq. (23) as

$$-l_4 s_{kn} + l_3 c_{kn} = k_5, \quad \text{where } k_5 = k_1 c_{hp} + k_2 s_{hp} - l_2. \tag{29}$$

Eq. (15) multiplied by s_{hp} is

$$l_2 c_{hp} s_{hp} - l_4 s_{hpkn} s_{hp} + l_3 c_{hpkn} s_{hp} = k_1 s_{hp}. \tag{30}$$

Eq. (16) multiplied by c_{hp} is

$$l_2 s_{hp} c_{hp} + l_4 c_{hpkn} c_{hp} + l_3 s_{hpkn} c_{hp} = k_2 c_{hp}. \tag{31}$$

Then, Eq. (31) subtracted from Eq. (30) is

$$-l_4 c_{kn} - l_3 s_{kn} = k_6, \quad \text{where } k_6 = k_1 s_{hp} - k_2 c_{hp}. \tag{32}$$

Next, Eq. (29) multiplied by l_3 is

$$-l_4 l_3 s_{kn} + l_3^2 c_{kn} = l_3 k_5. \tag{33}$$

Eq. (32) multiplied by l_4 is

$$-l_4^2 c_{kn} - l_3 l_4 s_{kn} = l_4 k_6. \tag{34}$$

Then, Eq. (34) subtracted from Eq. (33) is

$$(l_3^2 + l_4^2) c_{kn} = l_3 k_5 - l_4 k_6. \tag{35}$$

From Eq. (35),

$$c_{kn} = (l_3 k_5 - l_4 k_6)/(l_3^2 + l_4^2). \tag{36}$$

Eq. (29) multiplied by l_4 is

$$-l_4^2 s_{kn} + l_3 l_4 c_{kn} = l_4 k_5. \tag{37}$$

Eq. (32) multiplied by l_3 is

$$-l_3 l_4 c_{kn} - l_3^2 s_{kn} = l_3 k_6. \tag{38}$$

Then, Eq. (38) added to Eq. (37) is

$$-(l_3^2 + l_4^2) s_{kn} = l_3 k_6 + l_4 k_5. \tag{39}$$

From Eq. (39),

$$s_{kn} = (-l_3 k_6 - l_4 k_5)/(l_3^2 + l_4^2). \tag{40}$$

Therefore, from Eq. (36) and Eq. (40),

$$q_{kn} = \tan^{-1} \frac{s_{kn}}{c_{kn}} = \tan^{-1} \frac{-l_3 k_6 - l_4 k_5}{l_3 k_5 - l_4 k_6}. \tag{41}$$

REFERENCES

[1] A. M. Djuric, R. J. Urbanic, and J. L. Rickli, "A framework for collaborative robot (CoBot) integration in advanced manufacturing systems," *SAE Int. J. Mater. Manuf.*, vol. 9, no. 2, pp. 457–464, Apr. 2016.

[2] A. K. Pandey and R. Gelin, "A mass-produced sociable humanoid robot: Pepper: The first machine of its kind," *IEEE Robot. Autom. Mag.*, vol. 25, no. 3, pp. 40–48, Sep. 2018.

[3] M. Paolanti, M. Sturari, A. Mancini, P. Zingaretti, and E. Frontoni, "Mobile robot for retail surveying and inventory using visual and textual analysis of monocular pictures based on deep learning," in *Proc. Eur. Conf. Mobile Robots (ECMR)*, Sep. 2017, pp. 1–6.

[4] K. Miura, S. Nakaoka, S. Kajita, K. Kaneko, F. Kanehiro, M. Morisawa, and K. Yokoi, "Trials of cybernetic human HRP-4C toward humanoid business," in *Proc. IEEE Workshop Adv. Robot. Social Impacts*, Oct. 2010, pp. 165–169.

[5] *Dolce & Gabbana Used Drones to Carry Handbags Down the Runway Instead of Models*. Accessed: Jul. 10, 2021. [Online]. Available: https://www.theverge.com/tldr/2018/2/26/17052896/dolce-gabbana-drones-h%andbags

[6] N. Koyachi, T. Arai, H. Adachi, and A. Murakami, "Design and control of hexapod with integrated limb mechanism: MELMANTIS," in *Proc. IEEE/RSJ Int. Conf. Intell. Robots Syst. (IROS)*, Nov. 1996, pp. 877–882.

[7] N. Koyachi, T. Arai, H. Adachi, A. Murakami, and K. Kawai, "Mechanical design of hexapods with integrated limb mechanism: MELMANTIS-1 and MELMANTIS-2," in *Proc. 8th Int. Conf. Adv. Robotics. (ICAR)*, Jul. 1997, pp. 273–278.

[8] A. Roennau, G. Heppner, M. Nowicki, and R. Dillmann, "LAURON V: A versatile six-legged walking robot with advanced maneuverability," in *Proc. IEEE/ASME Int. Conf. Adv. Intell. Mechatronics*, Jul. 2014, pp. 82–87.

[9] I. Davliakos, I. Roditis, K. Lika, C.-M. Breki, and E. Papadopoulos, "Design, development, and control of a tough electrohydraulic hexapod robot for subsea operations," *Adv. Robot.*, vol. 32, no. 9, pp. 477–499, May 2018.

[10] B.-H. Jun, H. Shim, B. Kim, J.-Y. Park, H. Baek, S. Yoo, and P.-M. Lee, "Development of seabed walking robot CR200," in *Proc. MTS/IEEE OCEANS Bergen*, Jun. 2013, pp. 1–5.

[11] H. Shim, S.-Y. Yoo, H. Kang, and B.-H. Jun, "Development of arm and leg for seabed walking robot CRABSTER200," *Ocean Eng.*, vol. 116, pp. 55–67, Apr. 2016.

[12] D.-J. Lee, M. Park, and J.-H. Lee, "Height adjustable multi-legged giant Yardwalker for variable presence," in *Proc. IEEE Int. Conf. Adv. Intell. Mechatronics (AIM)*, Jul. 2015, pp. 104–109.

[13] A. A. M. Faudzi, G. Endo, S. Kurumaya, and K. Suzumori, "Long-legged hexapod Giacometti robot using thin soft Mckibben actuator," *IEEE Robot. Autom. Lett.*, vol. 3, no. 1, pp. 100–107, Jan. 2018.

[14] L. Chen, G. Zhong, Z. Liu, and H. Deng, "A novel hexapod robot: Design and mobility analysis," in *Proc. IEEE Int. Conf. Mechatronics Autom.*, Aug. 2016, pp. 2094–2098.

[15] M. Gorner, T. Wimbock, A. Baumann, M. Fuchs, T. Bahls, M. Grebenstein, C. Borst, J. Butterfass, and G. Hirzinger, "The DLR-crawler: A testbed for actively compliant hexapod walking based on the fingers of DLR-hand II," in *Proc. IEEE/RSJ Int. Conf. Intell. Robots Syst.*, Sep. 2008, pp. 1525–1531.

[16] M. Bjelonic, N. Kottege, T. Homberger, P. Borges, P. Beckerle, and M. Chli, "Weaver: Hexapod robot for autonomous navigation on unstructured terrain," *J. Field Robot.*, vol. 35, no. 7, pp. 1063–1079, Oct. 2018.

[17] L. Minati, M. Frasca, N. Yoshimura, and Y. Koike, "Versatile locomotion control of a hexapod robot using a hierarchical network of nonlinear oscillator circuits," *IEEE Access*, vol. 6, pp. 8042–8065, 2018.

[18] M. Travers, A. Ansari, and H. Choset, "A dynamical systems approach to obstacle navigation for a series-elastic hexapod robot," in *Proc. IEEE 55th Conf. Decis. Control (CDC)*, Dec. 2016, pp. 5152–5157.

[19] B. Tam, F. Talbot, R. Steindl, A. Elfes, and N. Kottege, "Open-SHC: A versatile multilegged robot controller," *IEEE Access*, vol. 8, pp. 188908–188926, 2020.

[20] D. Belter and P. Skrzypczyński, "A biologically inspired approach to feasible gait learning for a hexapod robot," *Int. J. Appl. Math. Comput. Sci.*, vol. 20, no. 1, pp. 69–84, Mar. 2010.

[21] *Mounting and Installation Guidelines*. Accessed: Jul. 10, 2021. [Online]. Available: https://www.kollmorgen.com/sites/default/files/Framless%20motor%20Mount%ing%20%26%20Installation%20Guidlines.pdf

SANGSIN PARK received the B.S. degree in mechanical engineering from Inha University, Incheon, South Korea, and the M.S. and Ph.D. degrees in mechanical engineering from Korea Advanced Institute of Science and Technology (KAIST), Daejeon, South Korea, in 2005, 2007, and 2017, respectively. He was a Postdoctoral Researcher with the Department of Mechanical Engineering, University of Nevada at Las Vegas, from 2017 to 2019, and a Principal Researcher with Rainbow Robotics, Daejeon, in 2019. He is currently a Team Leader with the Lab Division, IICOMBINED, Seoul, South Korea. His research interests include walking and control of legged robots.